

# **Nuclear Circuits and Systems**

## LOW-NOISE WIDE-BAND AMPLIFIER SYSTEM FOR STOCHASTIC BEAM COOLING EXPERIMENTS

Branko Leskovar and C. C. Lo  
Lawrence Berkeley Laboratory  
University of California  
Berkeley, California 94720 U. S. A.

Abstract

A new low-noise wide-band power amplifier system has been developed for stochastic beam cooling experiments. The system incorporates a low-noise preamplifier with a noise figure of 1.9 dB over a bandwidth range of 20 to 300 MHz, wide-band driver and buffer stages, a frequency characteristics shaping network, a remotely controlled wide-band attenuator with 0.1 dB resolution, a remotely controlled high resolution adjustable delay line, and a wide-band solid-state output power amplifier. The amplifier system has a maximum voltage gain of 140 dB over a bandwidth from 1.5 to 310 MHz, a signal group delay of 55.5 ns, and a c. w. output power level of 75 W. Particular attention was paid to minimizing the signal propagation time delay of the amplifier system, the propagation time delay change as a function of the system gain, and harmonic and intermodulation distortions. Using a new wide-band electron bombarded semiconductor output amplifier, the system will have a bandwidth from 30 to 400 MHz, a signal group delay of 37 ns and an output power of 100 W.

Introduction

Stochastic beam cooling is the gradual reduction of betatron oscillations or longitudinal momentum spread of a coasting particle beam by a wide-band feedback system<sup>1-2</sup>. The system detects and corrects at every revolution the statistical fluctuations of the beam position or momentum. Consequently, the stochastic cooling and the electron cooling are important methods of increasing the phase space density of particle beams. One or both methods of beam cooling are essential in order to achieve high luminosity proton-antiproton colliding beam facilities<sup>3</sup>.

A general layout of a wide-band feedback system for stochastic beam cooling is shown in Fig. 1. For the reduction of the horizontal and vertical betatron oscillations, two identical systems are necessary. The system typically consists of a wide-band pickup electrode, able to detect horizontal or vertical statistical displacements of short sample of a coasting beam, a low-noise wide-band power amplifier and kicker electrode which applies a correcting signal to the same sample. The time delay of the correcting signal is adjusted so that each beam sample acts on itself. This process is repeated continuously as the beam passes the pickup electrode. For the reduction of the longitudinal momentum spread, the system consists of a radial difference pickup electrode which observes the error in radial position of the barycentre of a short sample with respect to nominal radial position, a low-noise wide-band power amplifier and a wide-band accelerating/decelerating gap. The error generated by the pickup electrode is interpreted as a momentum error, and a fraction of it is corrected by amplifying the signal and applying it to the gap at the instant when the same sample passes<sup>4</sup>. In an alternate system for the momentum cooling<sup>5-6</sup> the pickup electrode signal after preamplification passes through a filter which changes its phase polarity characteristics at each harmonic of nominal revolution frequency that corresponds to a nominal

momentum. The amplified filtered signal is applied to a series of wide-band accelerating/decelerating gaps. Beam particles are accelerated or decelerated depending upon their momentum with respect to the nominal momentum. This method is particularly suitable for fast cooling at low beam intensities, because the signal-to-noise ratio remains high and it is independent upon beam radial position. The filter mentioned above is inserted in the wide-band power amplifier system. It follows the low-noise preamplifiers and attenuates much of the preamplifier noise.

Theoretical considerations and experimental results of the stochastic cooling have shown<sup>7-9</sup> that the effective cooling rate is limited by the feedback system bandwidth, the noise figure, the beam Schottky noise, the system gain, the power level available to the kicker electrode, the particle mixing process, imperfect filters and undesirable system phase shift errors.

The stochastic cooling program at the Lawrence Berkeley Laboratory<sup>10</sup> has created a need for the development of a low-noise wide-band amplifier system being capable of operating at output power levels higher than 70 W across a frequency bandwidth as wide as possible. Since the pickup electrode signal power levels from the particle beam are of the order of magnitude of

$0.5 \times 10^{-12}$  W, the amplifier system should have a gain in excess of 140 dB and a noise figure as low as possible. Furthermore, the system should have an accurately controllable signal propagation time delay. Also, the propagation time delay change as a function of the system gain settings, and harmonic intermodulation distortions should be minimized. Based on our previous considerations<sup>11</sup>, a new system has been designed to meet the above given requirements for fast cooling of betatron oscillations and longitudinal momentum spread. The present system characteristics are limited by capabilities of available individual state-of-the-art components. This amplifier system will be used as a part of the beam cooling facility at the Fermi National Accelerator Laboratory.

Description of the Low-Noise Wide-Band Amplifier System

A block diagram of the low-noise wide-band amplifier system is shown in Fig. 2. The system presently consists of the following components: a radio frequency electromechanical coaxial switch, a low-noise wide-band preamplifier, two wide-band amplifiers, an in-phase power divider, a 20 dB attenuator or frequency characteristic shaping network, a wide-band buffer amplifier, 0.1 dB, 1 dB and 10 dB step attenuators, a variable delay line, a wide-band driver amplifier, an out-of-phase power divider, two 35 W wide-band output power amplifiers, and two output radio frequency coaxial switches.

The electromechanical coaxial switch serves the following purposes: (1) to connect the pickup electrode to the input of the low-noise preamplifier, (2) to provide an input port to the preamplifier for system checking and calibration and (3) to disconnect the

preamplifier input from the pickup electrode. The coaxial switch can be locally and remotely controlled. After the pickup electrode signal has been amplified by 64 dB, it is applied to the frequency characteristic shaping network, or a 20 dB attenuator, via one port of the in-phase power divider. The amplified pickup electrode signal is available directly from the other port of the in-phase power divider for monitoring and diagnostic purposes. The frequency characteristic shaping network is used to make necessary correction to the pickup and kicker electrodes frequency responses. The average attenuation of the shaping network is approximately 17 dB. Whenever the shaping network is not in use, a 20 dB wide-band attenuator is inserted between the in-phase power divider and the wide-band buffer amplifier. The buffer amplifier provides a gain of 32 dB. Consequently, the total net gain from the input of the low-noise preamplifier and the output of the buffer amplifier is in the order of 70 dB. Assuming an input signal level of 5  $\mu$ V at the input of the preamplifier, the output signal level of the buffer amplifier will be 15 mV, which is well inside the linear operating range of this amplifier section. The signal propagation time delay through this section and the frequency bandwidth is 5.5 ns  $\pm$  0.2 ns and 1.5 - 500 MHz, respectively. The coaxial switch, the amplifiers, the in-phase power divider and the frequency characteristic shaping network are housed in a silver-plated copper box which is assembled directly on top of the pickup electrode.

If the amplifier system is used for the cooling of horizontal or vertical betatron oscillations, the output signal from the buffer amplifier is directly applied to the 129 dB attenuator which can be locally and remotely controlled. The attenuator can be controlled in 0.1 dB, 1 dB and 10 dB steps. The operating bandwidth of this attenuator is DC - 1 GHz. The change in the signal propagation time due to any setting of the attenuator is  $\pm$  0.07 ns in the worst case. If the amplifier system is used for the stochastic cooling of the longitudinal momentum spread the direct connection between the buffer amplifier and the attenuator is interrupted at point A in Fig. 2, and a filter network is inserted between the points a and b. A periodic notch filter is particularly suitable for this purpose. A low-loss- $\lambda/2$ -shorted cable has been used as this filter. It consists of an air-dielectric 7/8" diameter Helix cable, which has a velocity of 91.62% and a loss factor of 2 dB/100 m at 200 MHz, and yields notches with a maximum attenuation of 44 dB, 26 dB, and 17 dB at 2.5 MHz, 120 and 300 MHz, respectively. Because for an effective beam cooling, the signal propagation time from the pickup to kicker electrode should be equal to the particle's traveling time, the signal from the step attenuator is applied to an adjustable delay line before it is applied to the driver amplifier to obtain the required fine delay adjustment. The line section consists of two 1.6 ns fixed delay adjustments and one  $\pm$  0.8 ns variable delay line adjustments. The variable delay line resolution is better than 0.05 ns. The output signal from the adjustable delay line is amplified 34 dB by a solid state driver amplifier having a bandwidth of 0.002-400 MHz. The minimum signal propagation time through the driver amplifier section is 18 ns  $\pm$  0.2 ns. The output signal from the driver amplifier is applied to the out-of-phase power divider. To prevent any unintentional high input signals at the input of the amplifier system causing damage to the input stages of the output power amplifiers, an overloading circuit has been built into the driver amplifier stage. As the output of the driver amplifier stage approaches a level of 1V (the maximum input signal level for the output power amplifiers), this circuit will activate and interrupt the signal path at the input of the driver amplifier. This circuit must be reset manually to restore normal operation. The same

circuit is used to manually interrupt the signal path for checking purposes.

The kicker electrode design of the present feedback system for the stochastic cooling employs a push-pull configuration having a 0 degree and a 180 degree input. Since each output power amplifier is capable of delivering 35 W of linear power, the push-pull configuration provides a total of 70 W. The 3 dB amplitude bandwidth of these amplifiers is 150 KHz-310 MHz with a 45 degree phase lag at 250 MHz. The signal propagation time through the output power amplifiers is 32.2 ns  $\pm$  0.2 ns.

The output of these two amplifiers can be disconnected from the kicker electrode by a radio frequency electromechanical coaxial switch for diagnostic and tune-up purposes. An automatic protection circuit has been incorporated at the output of these amplifiers so that when the reflected power approaches 5 W, the output of the amplifiers would be connected automatically to two internal wide-band radio frequency loads. Resetting is automatically done in approximately 10 seconds, reapplying the output to the external loads. If the mismatch persists the output power amplifiers will operate in this mode indefinitely until the mismatch is removed.

At the present stage of development of the amplifier system, all amplifiers in the system are of solid-state design. The signal propagation time of the entire amplifier system excluding any interconnecting cable is 55.5 ns which is very close to the maximum allowable limit for a system for the reduction of betatron oscillations. Significant improvements can be achieved when an output power amplifier with better phase and amplitude bandwidth becomes available. A possible candidate is an Electron-Bombarded-Semiconductor, EBS, amplifier<sup>12</sup>. Under investigation is one such amplifier with a 30-400 MHz bandwidth capable of providing 100 W. Its phase-shift characteristics are expected to be better than  $\pm$  10 degrees over the entire bandwidth. Furthermore, the signal propagation time delay will only be about half of the present power amplifier.

The gain, however, of such an amplifier is typically 17-18 dB making it necessary to provide more driving power at the amplifier input. The higher power, wider bandwidth and shorter propagation time would undoubtedly make the amplifier system more efficient, providing a higher cooling rate of the beam cooling process. The associate support system for such an amplifier is, however, more complex than that for the solid state amplifiers. Also, an isolator is necessary between the output of the EBS device and the kicker electrode if there is a significant variation of the kicker electrode impedance through the frequency band.

The overall configuration of a deflection modulated EBS is shown in Fig. 3. The electron gun produces a broad, narrow sheet beam of electrons of energy 12-15 KeV, which is focused onto the semiconductor target. The radio frequency input signal is applied to a pair of traveling-wave deflection structures which act to deflect the electron beam proportional to the amplitude of the input signal. The diodes are reverse biased below their avalanche threshold. The diodes are interconnected in a class AB circuit with diodes on either side of the electron beam being excited during one half of radio frequency period. With no input signal applied, the electron beam with sharply defined planar beam edge is intercepted between the two sets of diodes. With the input signal applied, the fraction of the beam current is intercepted by the semiconductor diode. The electrons penetrate through the diode junction generating an amplified current in the high field region by impact ionization. For typical devices, the current multiplication in semiconductor target is 3000:1. Since

the output current is directly proportional to the current of the electron beam, the EBS device operates like a highly linear amplifier. An electrical matching network is provided to transform the semiconductor target impedance to a 50 Ohm output level. Because of the very short signal propagation time delay of the EBS power amplifier, the device is particularly suitable for stochastic cooling amplifier systems. Furthermore, with future improvements in areas of semiconductor diode cooling and output matching structure, the device frequency bandwidth and output power level will be significantly increased.

#### Dynamic Range and Intermodulation Products Measurement

The dynamic range measurement of the entire amplifier system shows the performance characteristics such as the linearity, gain, harmonic interference, and the intermodulation performance which can be expected from the amplifier at certain specified frequencies. Figure 4 shows a block diagram of the measuring system. The two signal generators were used only for intermodulation measurements. Three sample frequencies were used in the measurement; 5 MHz, 50 MHz and 120 MHz. Results at all three frequencies shows that the amplifier system has its 1 dB compression point at an output power close to 48 dBm ( $\approx 60$  W) and at 45.5 dBm ( $\approx 35$  W) which is the specified linear output power level, the second harmonic interference is 20 dB below the fundamental component. Figs. 5 and 6 show the typical results of the measurement with operating frequencies of 50 MHz and 120 MHz, respectively. Figure 7 is the output spectrum displayed on a spectrum analyzer. The marker was set at the peak of the second harmonic, and the fundamental power output was 45.5 dBm (35 W).

The amplifier system frequency response was also measured using usual measuring technique. The system normalized gain for  $0^\circ$  and  $180^\circ$  outputs as a function of frequency is given in Fig. 8. It can be seen from the figure that the 3 dB bandwidth is 1.5 MHz-310 MHz.

#### Phase-Shift Characteristic Measurement

The phase-shift characteristics of the amplifier system are important for proper operation of the wide-band feedback cooling system both from the stand point of overall system stability and to allow an estimate of the phase-shift error between the pickup and kicker electrode signals. Too great a phase-shift error causes the heating of the particle beam. The phase-shift characteristic was measured using the measuring system shown in Fig. 9.

The pulse generator was first used to adjust the signal propagation time of the delay cable to be equal to that of the amplifier system and associated components by observing amplified and cable pulses displayed on the oscilloscope. The signal generator was then connected in place of the pulse generator and the two output signals were transferred to the vector voltmeter from the oscilloscope. A 200 MHz signal was used to fine tune the signal paths, at which frequency the phase angle between the two output signals was adjusted to zero. By varying the input signal frequency, the phase angle change was measured as a function of frequency and the result shown plotted in Fig. 10. The measurement was made for both the  $0^\circ$  and  $180^\circ$  amplifier channels. From Fig. 10 the phase variation is seen to be  $\pm 22.5^\circ$  over a bandwidth of 10-220 MHz.

#### Voltage Standing-Wave Ratio Measurement

The input Voltage Standing-Wave Ratio, VSWR, was measured at the input of the amplifier system which included the radio frequency coaxial switch at the input. The output VSWR was also measured with the output coaxial switch and line section in the circuit. A transmission/reflection test set up was used for this measurement as shown in Fig. 11.

A signal generator was used to generate the signal frequency of interest. A power splitter was used to divide the signal into two equal parts. One part was used as the input reference. The other part was used as a test signal.

The signal path from point R to point A was equal to that from point S through the test port and to point B. A directional coupler was used to isolate the incident signal and to separate out the observed reflected signal from the test port. The reflection coefficient was found from the incident and reflected signal, and a Smith Chart was used to determine the VSWR. The input VSWR was measured across the 1.2-425 MHz bandwidth at a power level of 20  $\mu$ W. The output VSWR was measured across 1.2-350 MHz bandwidth at the two power levels, 200  $\mu$ W and 0.5 W, yielding similar results. The result of the measurements are given in Fig. 12. The maximum VSWR of the input is 1.58 at 1.2 MHz and 375 MHz while the maximum output VSWR of 1.9 and 1.97 occur at 300 MHz for the  $180^\circ$  and  $0^\circ$  channel, respectively.

#### Pulse Response Measurement

The particle beam cooling process can be analyzed and modeled either in the time domain or in the frequency domain. For the time domain analysis, it is important to know the pulse response of the amplifier system. The system pulse response was measured using a 1 ns, FWHM, input pulse. The input pulse amplitude was adjusted so that the amplifier output pulse had a peak power of approximately 18 W. As is shown in Fig. 13, the 1 ns input pulse, (upper trace) was stretched to 3 ns, FWHM, output pulse with approximately 8 cycles of 330 MHz ringing following the main pulse (lower trace). The amplifier system response was also measured using 120 MHz and 300 MHz bursts as input signals. The waveform of the 120 MHz input RF burst (lower trace) and the output burst (upper trace) are shown in Fig. 14. The output radio frequency burst waveform at this frequency had nearly the same waveform as the input pulse. In Fig. 15 similar burst waveforms, but at 300 MHz, which is very close to the upper limit of the amplifier system frequency response, are shown. At this frequency, the output waveform burst required 28 ns to reach its peak value. The output waveform recovery time was also 28 ns.

#### Noise Consideration of the Amplifier System

The particle beam cooling process is characterized essentially by the following effects: (1) the coherent effect where each beam sample cools itself via the feedback system by the signal it generates and (2) the incoherent effect, where the beam heats itself because of the noise generated by the other beam particles (beam Schottky noise) and the presence of the noise of the amplifier system. The coherent effect is proportional to the amplifier system gain. The incoherent effect varies with the square of the gain. Consequently,

it is always possible to select a value of the system gain where the coherent effect is predominant and beam cooling is achieved. For low intensity particle beams such as in the FNAL cooling ring facility, with  $10^7$  particles ( $\approx 1 \mu A$ ), the heating effect will be dominated by the amplifier system noise rather than beam noise. Also, during the cooling process the ratio of the amplifier system noise power to the signal noise power increases continuously and the instantaneous cooling rate is reduced accordingly. Consequently, the cooling system could have considerably larger cooling rate dynamic range if an amplifier system with a lower noise figure is used.

The function of the low-noise, high-gain, wide-band power amplifier system is to amplify pickup electrode signals and to filter them in a manner that will provide the maximum discrimination between the desired signal and undesired noise and interference. The noise and interference comprises not only that generated in the low-noise preamplifier, but also spurious signals generated from fundamental and non-fundamental sources in the pickup electrode and its terminating resistor.

The usual noise that exists in a low-noise power amplifier is partly of thermal origin and partly due to other noise generating processes. Generally, the noise of a low-noise power amplifier is characterized either by the effective input noise temperature  $T_e$ , defined as  $T_e = P_n / k \Delta f$ , where  $P_n$  is the available noise power,  $k$  is Boltzman's constant and  $\Delta f$  the bandwidth, or by the noise figure  $F$ . The relationship between the noise figure  $F$  in dB and effective noise temperature is given by:

$$T_e = 290 \left( 10^{F_{dB}/10} - 1 \right) \quad (1)$$

The low-noise power amplifier system under consideration consists of a very low-noise preamplifier, driver and buffer stages, various electronic components and circuits, and an output high power stage. The amplifier system performance with respect to the system operating noise temperature  $T_{op}$  and the dynamic range is primarily determined by its front end characteristics.

The most meaningful measure of overall amplifier sensitivity where the amplifier is to be used in a pickup electrode-amplifier system is the system operating noise temperature  $T_{op}$  defined (under actual operating conditions) by the equation:

$$T_{op} = T_a + T_e^* \quad (2)$$

where  $T_a$  is the noise temperature of the pickup electrode, representing the available noise power at the pickup electrode terminals, and  $T_e^*$  is the effective input noise temperature of the amplifier system<sup>13</sup>. Each component in the amplifier front end cascade has its own effective input noise temperature  $T_e$ , representing its available output noise power referred to its own input terminals, assuming a noise free input terminal of the same impedance as the actual input termination. For an N-component cascade, the system operating noise temperature is given by the expression:

$$T_{op} = T_a + \sum_{i=1}^N \frac{T_e(i)}{G_i} \quad (3)$$

where  $G_i$  is the available gain of the system between its input terminals and the input terminals of the  $i$ th component. (By this definition,  $G_1 = 1$ ).

The formula given above can be applied to the pickup electrode-low-noise power amplifier-kicker electrode system representing the typical arrangement for stochastic cooling in a colliding beam facility. A block diagram of the cascade system used as a basis of system-noise-temperature calculations is shown in Fig. 16. The first component is the pickup electrode followed by the transmission line that connects the pickup electrode to the electromechanical radio frequency coaxial switch input terminals. Coaxial switch, having temperature  $T_{sw}$  and insertion loss factor for  $L_{sw}$ , is followed by the transmission line which connects the switch to the low-noise preamplifier input terminals. For this system, if the first transmission-line noise temperature is represented by  $T_{ra}$  and its loss factor is  $L_{ra} (= 1/G_{ra})$ , the coaxial switch noise temperature is  $T_{sw}$  and its loss factor  $L_w$ , the second transmission line noise temperature is  $T_{rb}$  and its loss factor  $L_{rb} (= 1/G_{rb})$ , and if the amplifier system effective input noise temperature is  $T_e$  at preamplifier input terminals, Equation (3) becomes:

$$T_{op} = T_a + T_{ra} + L_{ra} T_w + L_{ra} L_w T_{rb} + L_{ra} L_w L_{rb} T_e \quad (4)$$

The transmission line loss factor  $L_r$ , is defined as a ratio of the signal power available at its input to that available at its output.

It can be shown that the transmission lines noise temperature can be expressed by the equation:

$$T_{ra} = T_{tra} (L_{ra} - 1) \quad (5)$$

$$T_{rb} = T_{trb} (L_{rb} - 1) \quad (6)$$

where  $T_{tra}$  and  $T_{trb}$  are the transmission lines thermal temperatures.

A comparison of the pickup electrode noise with the effective input noise temperature of the amplifier front end shows that the pickup electrode noise can contribute significantly to the total system operating noise and may ultimately limit the achievable cooling system effectiveness, such for example as the cooling rate and time.

It is obvious from Equation 2 that in the case  $T_e^* \ll T_a$ , the cooling effectiveness of the pickup electrode-amplifier system cannot be significantly improved since the pickup electrode would introduce thermal noise into the amplifier system. The pickup electrode noise temperature would dominate the total noise temperature of the system. However, our investigation has shown<sup>11</sup>, that in the present system  $T_a \ll T_e^*$ , and that

future effort should be directed toward reducing the effective input noise temperature of the low-noise pre-amplifier stage. Consequently, in the pickup electrode-amplifier system the optimum tradeoff between the sensitivity, complexity, reliability, and cost occurs when the level of the amplifier front end effective noise temperature  $T_e^*$  is comparable to the pickup electrode noise temperature  $T_a$ , i.e.  $T_e^* \approx T_a$ .

The noise figure of the amplifier system was measured as a function of frequency using conventional measuring technique. The results of the measurement are given in Fig. 17. The accuracy of the measurement was  $\pm 0.15$  dB after all necessary corrections were taken into account. The measuring results include the losses of the electromechanical coaxial switch, and the switch input and output transmission lines.

### Conclusions

Design and performance characteristics of a low-noise wide-band high-gain amplifier system for a stochastic particle beam cooling facility have been presented and discussed. Particular attention was paid to minimize the signal propagation time delay of the system, the propagation time delay change as a function of the system gain, and harmonic and intermodulation distortions. The system was designed in a modular form and can be easily modified by increasing the bandwidth and power of the output power amplifiers. Future improvements will include further reduction of the amplifier system noise figure, operating the preamplifier, and other front end components at cryogenic temperatures.

In a final configuration at the FNAL beam cooling facility, two identical amplifier systems will be used for fast cooling of betatron oscillations, and one system with notch filter for cooling of the longitudinal momentum spread.

### Acknowledgments

This work was performed as part of the program of the Electronics Research and Development Group and the Advanced Accelerator Group of the Lawrence Berkeley Laboratory, University of California, Berkeley, and was supported by the Office of High Energy and Nuclear Physics of the U. S. Department of Energy under contract No. W-7405-ENG-48.

### References

1. H. G. Hereward, Statistical Phenomena-Theory, Proc. of the 1st Course of the International School of Particle Accelerators, Erice, 1976, CERN 77-13, pp. 281-289, July 1977.
2. W. Schnell, Statistical Phenomena-Experimental Results, Proc. of the 1st Course of the International School of Particle Accelerators, Erice, 1976, CERN 77-13, pp. 290-313, July 1977.
3. D. Möhl, Stochastic Cooling. European Organization for Nuclear Research Report CERN/PS/DL 78-25, October, 1978.
4. R. B. Palmer, Stochastic Cooling, Brookhaven National Laboratory Report, BNL-18395, Oct. 1973.
5. G. Carron, L. Thorndahl, Stochastic Cooling of Momentum Spread by Filter Techniques, CERN/ISR-RF-12, 1978.

6. G. Carron, H. Herr, G. Lebee, H. Koziol, F. Krienen, D. Möhl, G. Petrucci, C. Rubbia, F. Sacherer, G. Sadoulet, G. Stefanini, L. Thorndahl, S. van der Meer, T. Wikberg, Experiments on Stochastic Cooling in ICE. Report CERN-EP-179-16, March 1, 1979, Trans. of the IEEE 1979 Particle Accelerator Conf., San Francisco, March 12-14, 1979, Vol. NS-26, pp. 3456-3461, 1979.
7. S. van der Meer, Stochastic Cooling Theory and Devices, Proc. of the Workshop on Producing High Luminosity High Energy Proton-Antiproton Collisions March 27-31, 1979, Berkeley, California, Lawrence Berkeley Laboratory Report, LBL-7574, UC-34C, CONF-780345, pp. 73-77.
8. G. Carron, H. Herr, H. Koziol, F. Krienen, D. Möhl, G. Petrucci, C. Rubbia, F. Sacherer, B. Sadoulet, L. Thorndahl, S. van der Meer, T. Wikberg, Stochastic Cooling Tests in ICE, Physics Letters, Vol. 77B, No. 3, August 14, 1978.
9. F. J. Sacherer, Stochastic Cooling Theory, CERN-ISR-TH/78-11, 1978.
10. G. R. Lambertson, J. J. Bisognano, W. S. Flood, L. J. Laslett, C. W. Leeman, B. Leskovar, C. C. Lo, R. B. Main, L. Smith, Stochastic Cooling at the Fermilab Cooling-Ring, Lawrence Berkeley Laboratory Proposal, November 8, 1978.
11. B. Leskovar, Low-Noise Power Amplifier Considerations for Stochastic Cooling System, Lawrence Berkeley Laboratory Report LBL-9161, November 2, 1978, Presented at the Workshop for Producing High Luminosity-High Energy Proton-Antiproton Collisions March 27-20, 1978, Lawrence Berkeley Laboratory Berkeley, California.
12. D. J. Bates, R. I. Knight, S. Spinella, Electron-Bombarded Semiconductor Devices, Advances in Electronics and Electron Physics, Vol. 44, pp. 221-281, 1977.
13. B. Leskovar, D. B. Hopkins, W. F. Kolbe, Optimal Design Criteria for Millimeter-Wave Spectrometers Proc. of the 5th European Microwave Conference, Hamburg, pp. 228-232, September 1-4, 1975.

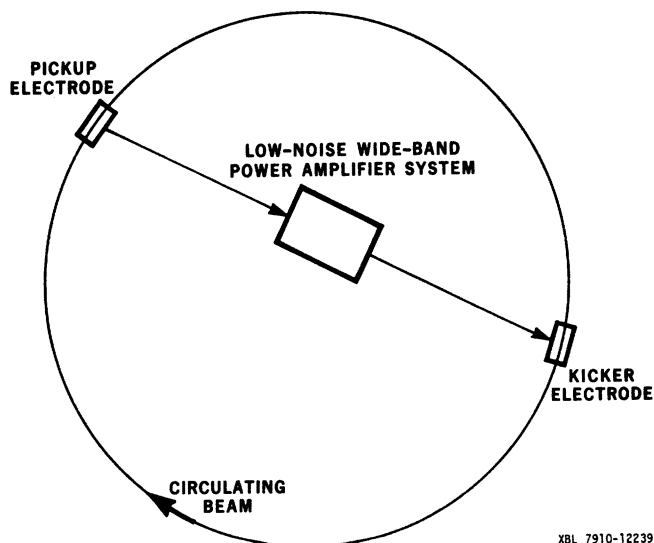


Fig. 1 Schematic representation of a circulating beam with stochastic cooling.

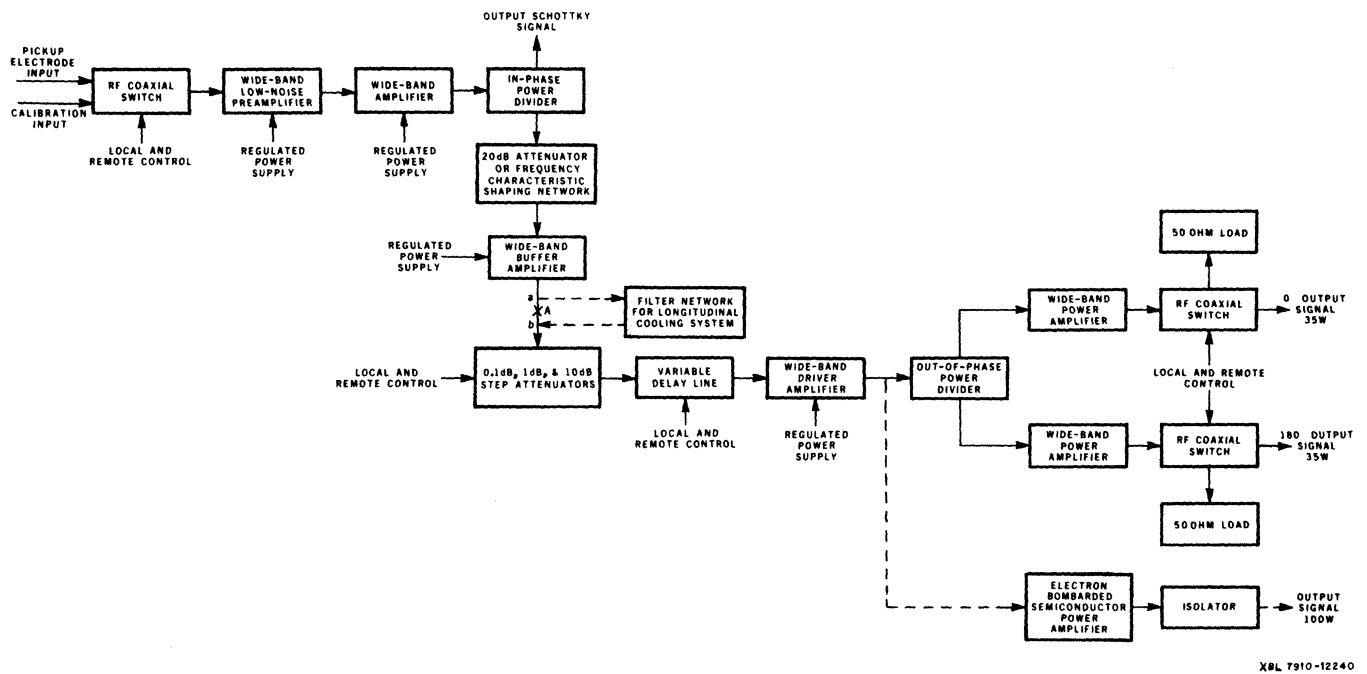


Fig. 2 Block diagram of the low-noise wide-band amplifier system for stochastic beam cooling experiments.

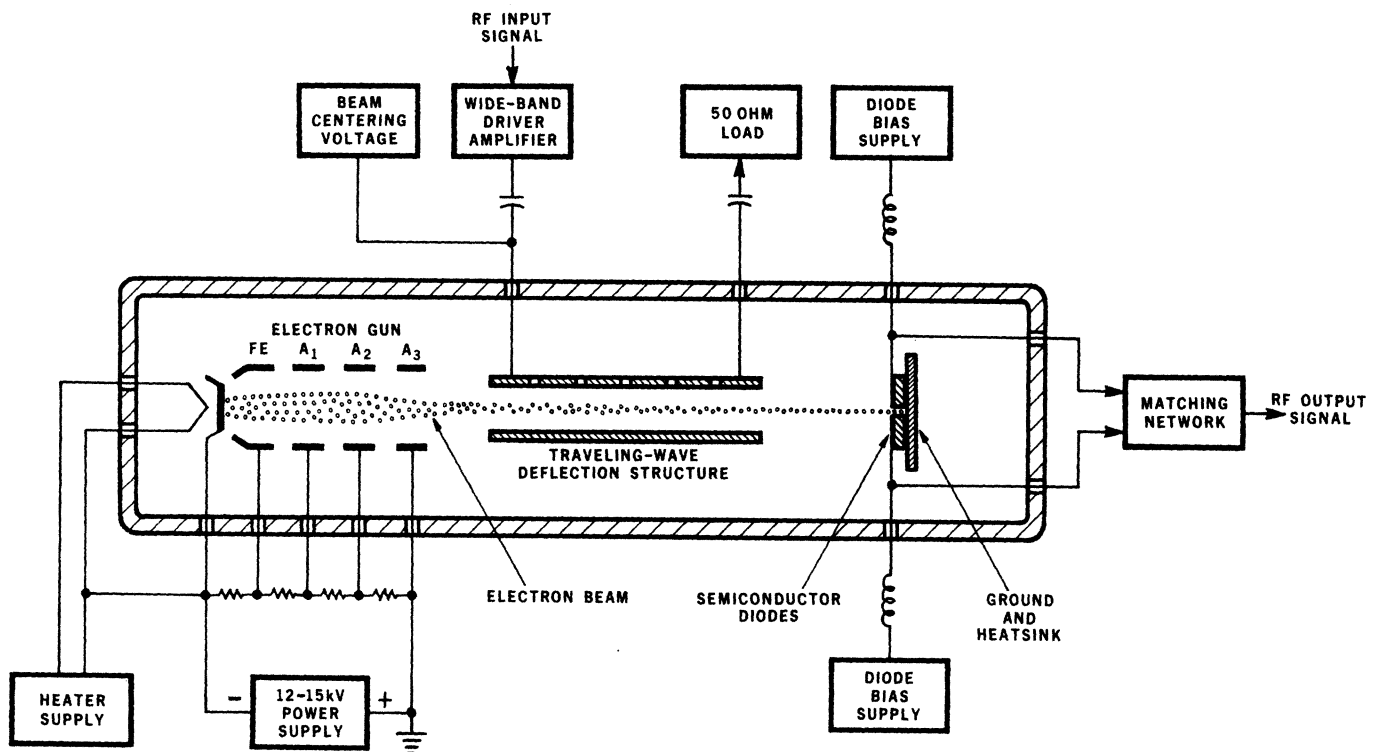
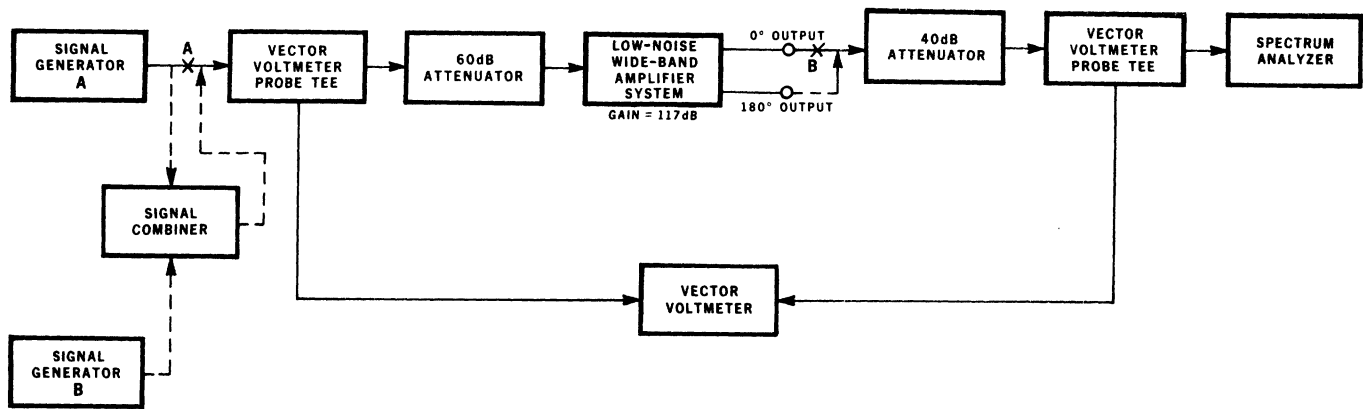
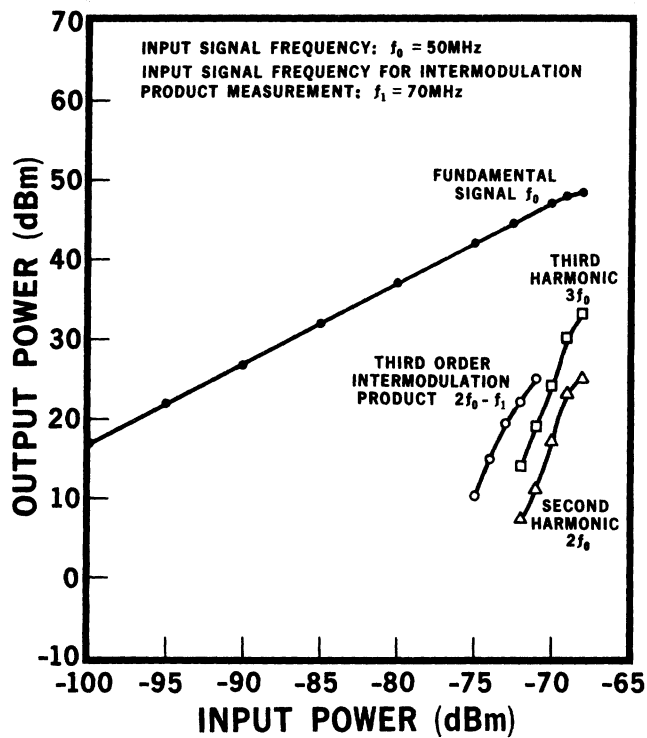


Fig. 3 Schematic arrangement of a deflection-modulated electron bombarded semiconductor amplifier.



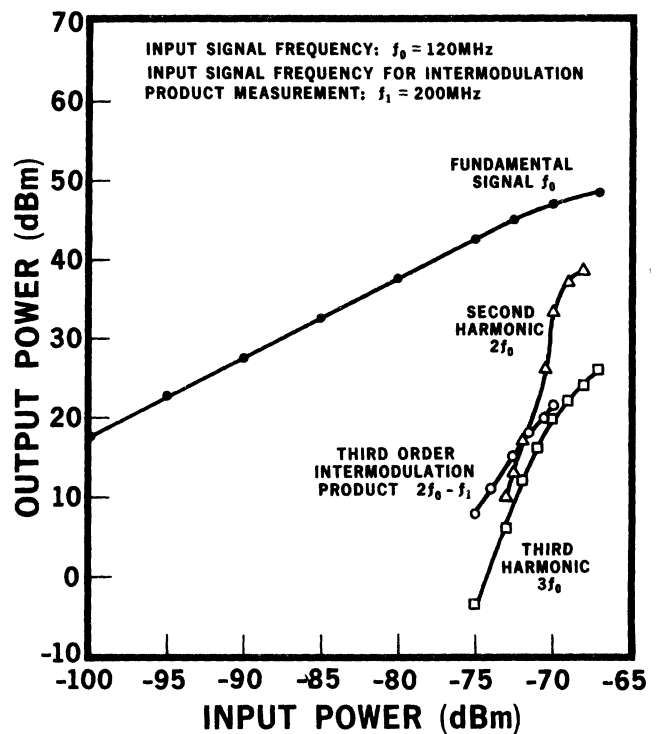
XBL 7910-12242

Fig. 4 System block diagram for dynamic range and intermodulation product measurements.



XBL 7910-12243

Fig. 5 Typical performance characteristics of the low-noise wide-band power amplifier system with an input signal frequency  $f_0 = 50$  MHz.



XBL 7910-12244

Fig. 6 Typical performance characteristics of the low-noise wide-band power amplifier system with an input signal frequency  $f_0 = 120$  MHz.



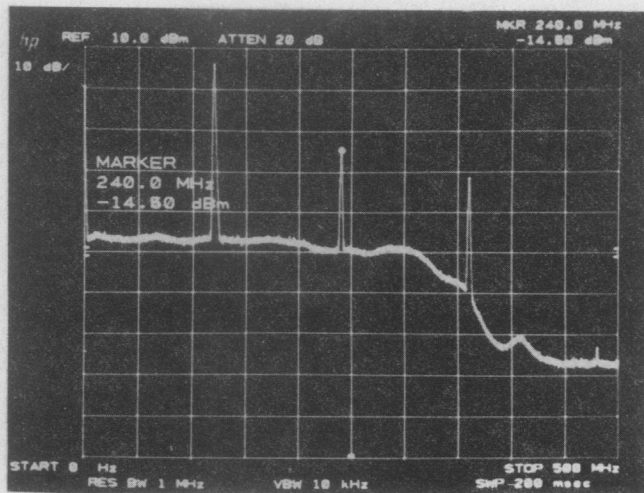


Fig. 7 Frequency spectrum display of the 120 MHz amplifier system output signal. The spectrum was taken with a spectrum analyzer having a 1 MHz resolution bandwidth across a frequency scan of 500 MHz.

$$f_0 = 120\text{MHz}$$

XBB 7910-13598

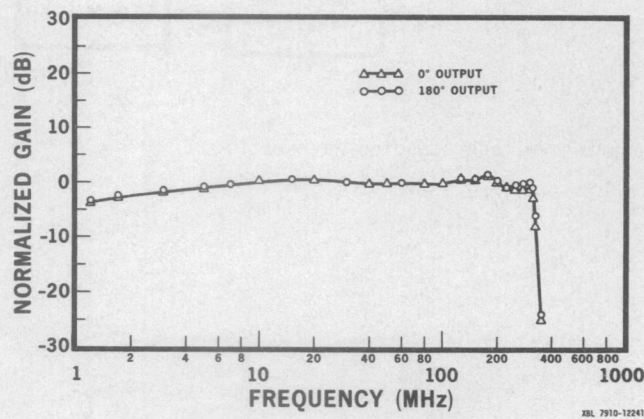


Fig. 8 Normalized gain as a function of frequency of the amplifier system.

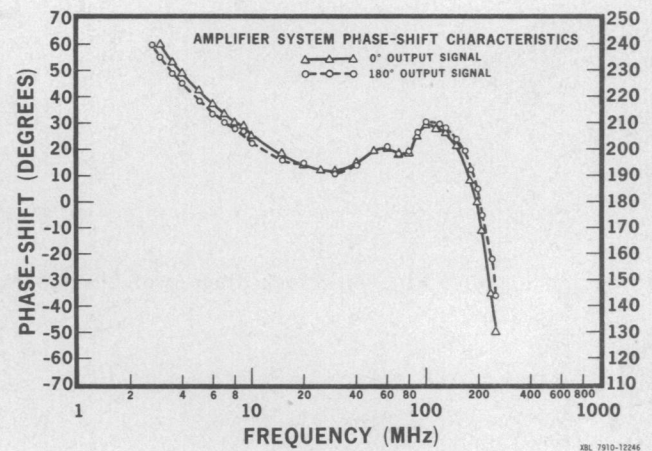


Fig. 10 Amplifier system phase shift characteristics.

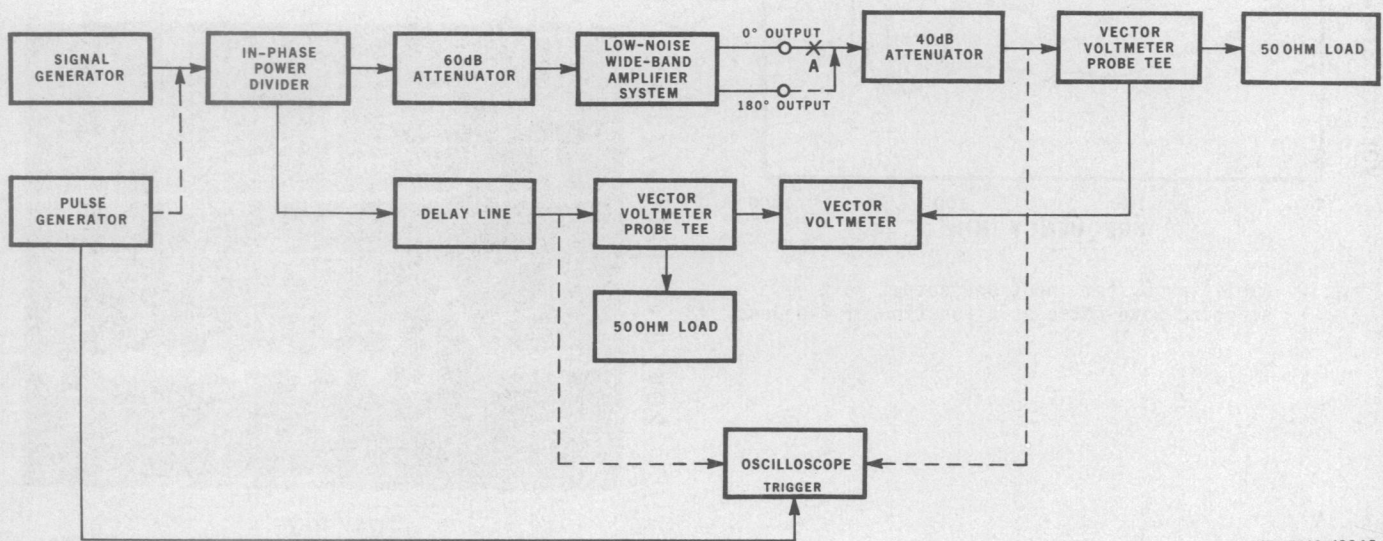
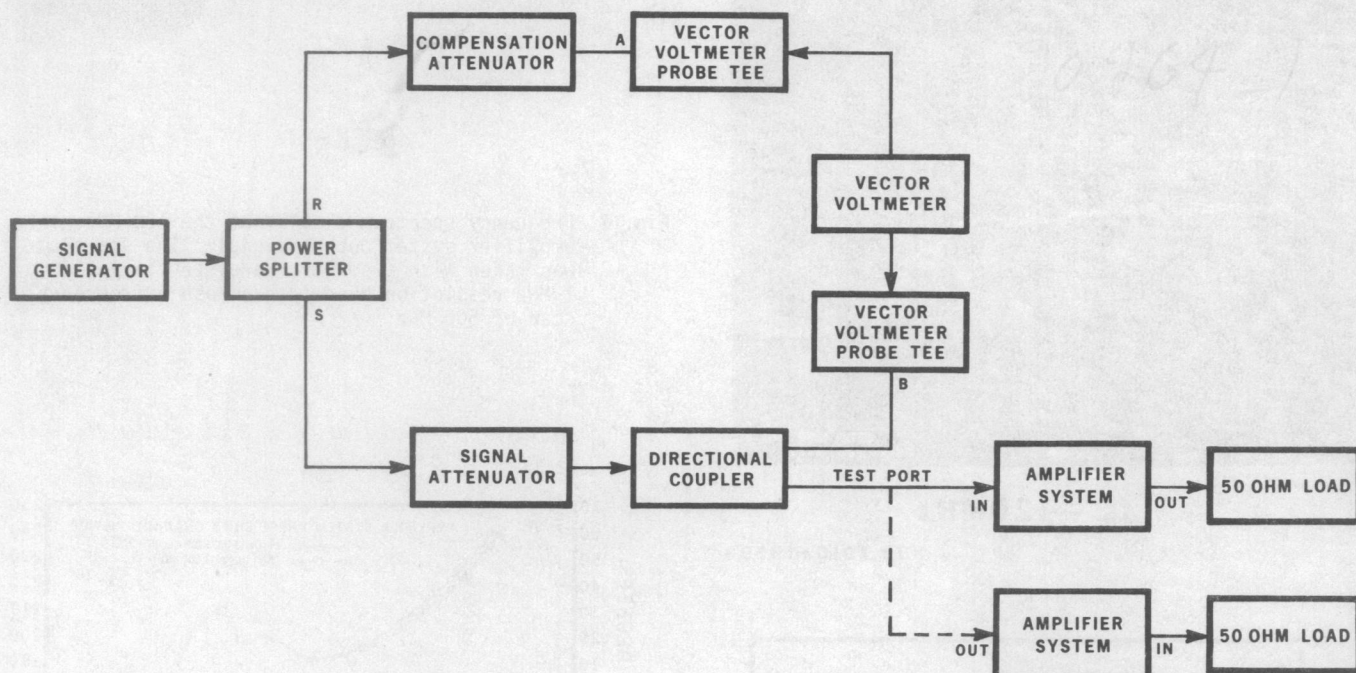
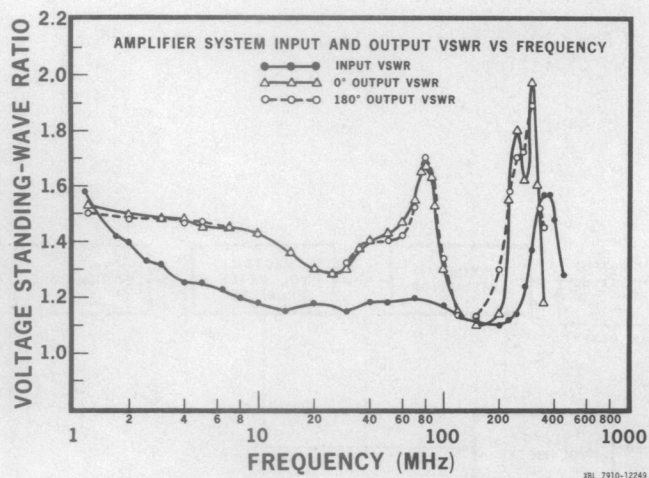


Fig. 9 Block diagram of the system for measuring amplifier phase-shift characteristics.



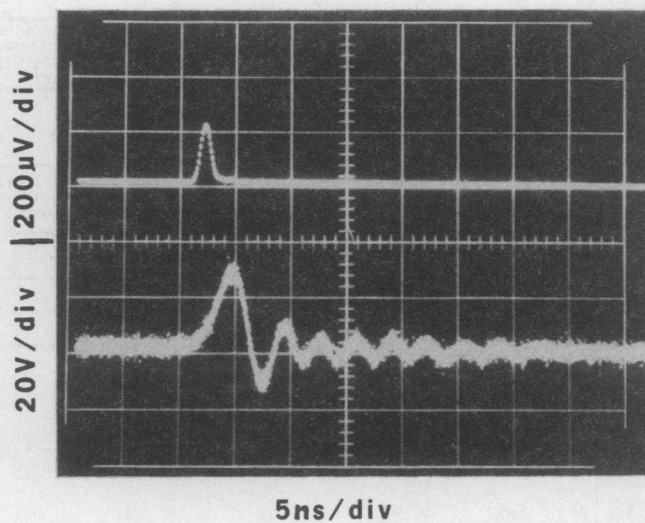
XBL 7910-12248

Fig. 11 Block diagram of the system for measuring voltage standing-wave ratio.



XBL 7910-12249

Fig. 12 Amplifier system input and output voltage standing-wave ratio as a function of frequency.



XBB 7910-13599

Fig. 13 Pulse response of the amplifier system.

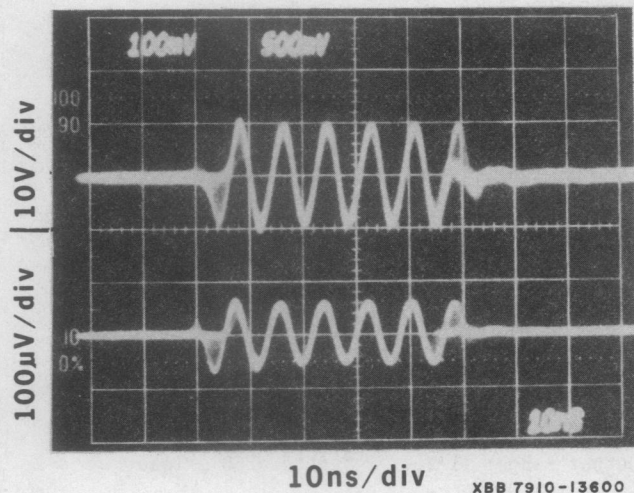


Fig. 14 The input and output waveforms from the amplifier system for a 120 MHz radio frequency burst.

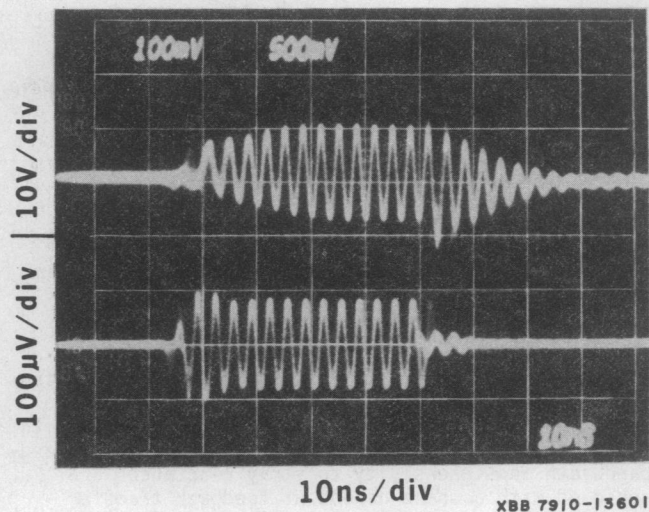


Fig. 15 The input and output waveforms from the amplifier system for a 300 MHz radio frequency burst.

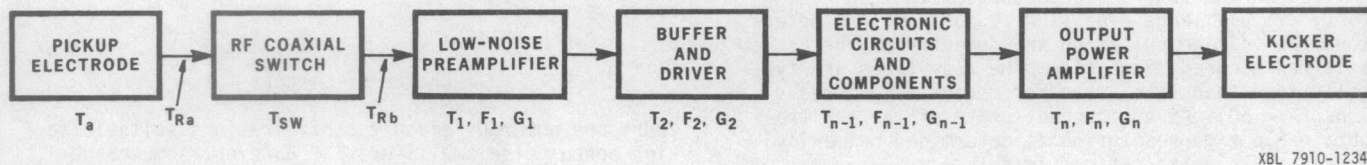


Fig. 16 Block diagram of the system used as a basis for noise temperature calculations.

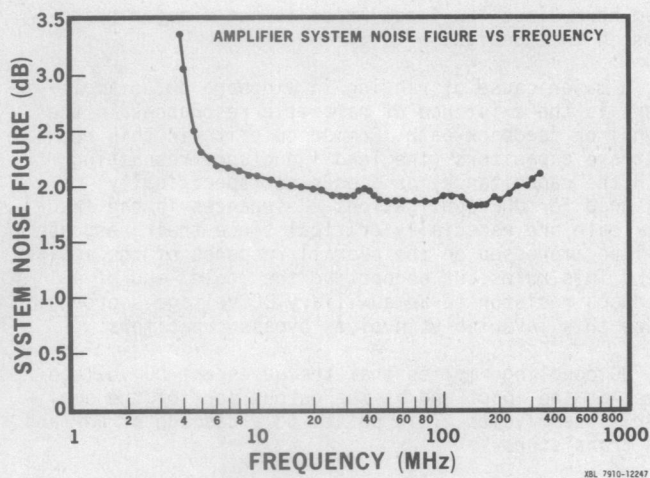


Fig. 17 Noise figure of the amplifier system as a function of frequency.